M–H–BR_3 and M–Br–BR_3 Interactions in Rhodium and Nickel Complexes of an Ambiphilic Phosphine-Thioether-Borane Ligand

*Bradley E. Cowie and David J. H. Emslie**

* Department of Chemistry & Chemical Biology, McMaster University, 1280 Main Street West, Hamilton, Ontario, L8S 4M1, Canada.

E-mail: emslied@mcmaster.ca. Tel: 1-(905)-525-9140 x 23307. Fax: 1-(905)-522-2509.

ABSTRACT

Reaction of [Rh(μ-Cl)(CO)(TXPB)] (**1**; TXPB = 2,7-di-*tert*-butyl-5-diphenylboryl-4-diphenylphosphino-9,9-dimethylthioxanthene) with $NaBH_4$ yielded square planar [Rh(μ-H)(CO)(TXPB)] (**2**) in which the hydride ligand bridges between rhodium and the borane unit of TXPB. The Rh–H, Rh–B and Rh–C_{ipso} distances are short {1.84(5), 2.456(6) and 2.568(5) Å, respectively}, whereas the B–H bond {1.59(6) Å} falls at the longer end of the usual range. Compound **2** is compared with the previously reported series of rhodium TXPB complexes: [RhX(CO)(TXPB)] {X = F (**3**), Cl (**1**), Br (**4**), I (**5**)}. Compound **4** in this series features the only crystallographically characterized example of an M–Br–BR_3 interaction, and to expand this area, [NiBr(μ-Br)(TXPB)] (**6**) was prepared via the reaction of [$NiBr_2(dme)_2$] (dme = 1,2-dimethoxyethane) with TXPB. An X-ray crystal structure of light purple **6** revealed a square-planar geometry with a strong B–Br interaction {B–Br = 2.311(6) Å; Σ(C–B–C) = 344.5(7)°}. An ^{11}B NMR chemical shift of 23 ppm was observed for **6**, indicating that an appreciable B–Br interaction is maintained in solution. No signals were observed in the $^{31}P\{^1H\}$ NMR spectrum at room temperature, whereas a broadened ^{31}P signal was observed at –20 °C, evolving into a sharp singlet at –67 °C. This behaviour suggests that at room temperature, square planar **6** exists in equilibrium with a paramagnetic tetrahedral isomer, present at a level below that detectable through Evans magnetic measurements.

Keywords: Ambiphilic Ligands, Pendant Boranes, Rhodium, Nickel, Bridging Ligands

Introduction

Early efforts in transition metal–borane chemistry were directed towards the synthesis and characterization of complexes featuring direct η^1*B*-coordination of a borane to the metal centre. Such complexes proved elusive for many years, and isolated unsupported examples (i.e. those in which the borane is not incorporated into an ambiphilic ligand framework) are limited to [(^{t}Bu$_3$SiO)$_3$Ta(BH$_3$)], for which η^1*B*- and η^2*BH*-coordinated isomers are predicted to be similar in energy.[1,2] The first structurally authenticated example of a transition metal complex bearing an η^1*B*-coordinated borane ligand was reported in 1999 by Hill and co-workers, who exploited an *in-situ*-generated ambiphilic ligand framework to promote ruthenium–borane coordination.[3] Since this early report, a considerable variety of borane-containing ambiphilic ligands have been developed and successfully deployed in the synthesis of transition metal complexes exhibiting either direct η^1*B*-coordination of the pendant borane, or delocalized η^{n+1}*BC*$_n$-coordination of an arylborane unit.[4,5]

A significant number of ambiphilic ligand complexes featuring M–Cl–BR$_3$ bridging interactions have also been prepared.[4] By contrast, complexes featuring M–Br–BR$_3$ and M–I–BR$_3$ bridging interactions are scarce, and to the best of our knowledge, crystallographically characterized examples are limited to [RhBr(CO)(TXPB)],[6] [RhI(CO)(TXPB)] and [PtI$_2$(TXPB)].[7] Previously we investigated the nature of the borane–halide and/or borane–metal interactions in the following TXPB complexes: (a) [RhX(CO)(TXPB)] (X = F, Cl, Br and I) and [Rh(CO)(TXPB)][PF$_6$] (Scheme 1),[6,8] and (b) [MX$_2$(TXPB)] (M = Pd or Pt; X = Cl or I).[7] These studies revealed halide abstraction by the borane in the case of X = F, a strong halide–borane interaction for X = Cl and Br, and a weak halide–borane interaction for X = I. Furthermore, upon abstraction of a halide co-ligand to generate cationic [Rh(CO)(TXPB)]$^+$, η^2*BC*-coordination of the arylborane unit was observed. These findings are consistent with the soft nature of rhodium(I), palladium(II) and platinum(II), and the moderately hard nature of the borane Lewis acid. Herein we extend this work to include [Rh(μ-H)(CO)(TXPB)] (**2**) and [NiBr(μ-Br)(TXPB)] (**6**).

Scheme 1. Synthesis of [RhX(CO)(TXPB)] (X = F, Cl, Br and I) and [Rh(CO)(TXPB)][PF_6].[6,8]

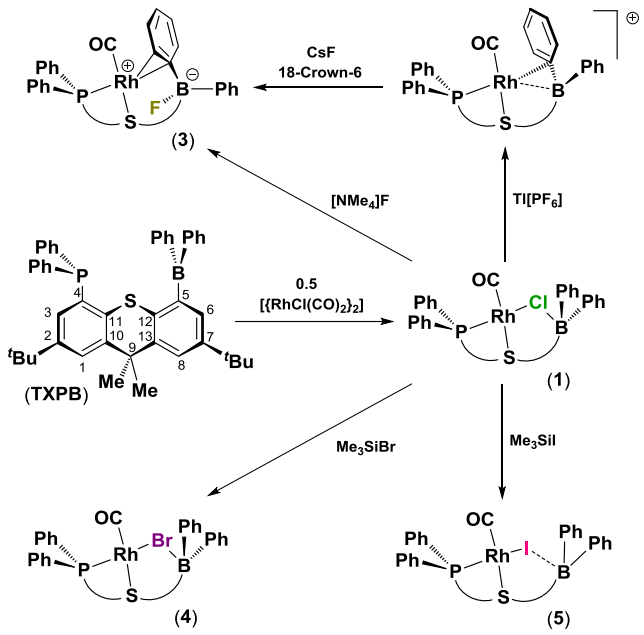

Compound **2** was targeted to allow direct comparison of a Rh–H–BR_3 interaction with Rh–X–BR_3 (X = F, Cl, Br, I) interactions. Several reactions of borane-containing ambiphilic ligand complexes which generate an M–H–BR_3 interaction have recently been reported. Peters and co-workers have exploited the {*o*-(Ph_2P)C_6H_4}$_2$BMes (^{Ph}DPB^{Mes}; Mes = C_6H_2-2,4,6-Me_3) ligand to prepare the nickel(0) complex, [Ni(^{Ph}DPB^{Mes})], which readily reacts with H_2 or silanes to provide [NiH(μ-H)(^{Ph}DPB^{Mes})] and [NiR(μ-H)(^{Ph}DPB^{Mes})] (R = SiH_2Ph, $SiHPh_2$), respectively, and has been shown to be capable of catalytic hydrogenation and hydrosilylation reactivity.[9] Additionally, Peters and co-workers have utilized {*o*-(^{i}Pr$_2$P)C_6H_4}$_3$B (^{iPr}TPB) in the generation of [Fe(N_2)(^{iPr}TPB)], which readily reacts with either one or two equivalents of H_2 to provide [Fe(N_2)(H)(μ-H)(^{iPr}TPB)] and [Fe(H_2)(H)(μ-H)(^{iPr}TPB)], respectively, or with CO and CN^{t}Bu to yield [FeL(^{iPr}TPB)] (L = CO, CN^{t}Bu), which undergo subsequent reactivity with H_2 to form [FeL(H)(μ-H)(^{iPr}TPB)] (L = CO, CN^{t}Bu) complexes; [Fe(N_2)(^{iPr}TPB)] is also capable of catalytic hydrogenation reactivity.[10] Furthermore, we previously reported a platinum(0) bisphosphine-borane complex, [Pt(FcPPB)] (FcPPB = [Fe(η^5-$C_5H_4PPh_2$)(η^5-$C_5H_4P^tBu${(*o*-BPh_2)C_6H_4})]), that readily reacted with H_2 to afford [PtH(μ-H)(FcPPB)],[11] with one terminally coordinated hydride ligand and one

bridging between platinum and the pendant borane. Beyond oxidative addition (of H_2 or HX) or electrophilic addition (of H^+) reactions, complexes featuring M–H–BR_3 interactions may be synthesized by hydroboration of a pendant vinyl group in a metal hydride complex,[12] reaction of a hydroborane with a metal-bound anionic ligand with multiple Lewis basic sites (e.g. CH_2PMe_2 or $NRP(OEt)_2$=O),[13-15] or substitution of a halide co-ligand for a hydride through the use of an alkali metal hydride or borohydride reagent;[16] the latter method has been deployed in the synthesis of **2**.

Compound **6**, [NiBr(μ-Br)(TXPB)], was targeted in order to study the extent to which the M–Br–BR_3 interaction is influenced by the "hardness" of the metal and potentially the coordination geometry, given that nickel(II) complexes may be either tetrahedral or square planar.

Results and Discussion

A rhodium(I) μ-Hydride Complex:

Reaction of [Rh(μ-Cl)(CO)(TXPB)] (**1**) with one equivalent of $NaBH_4$ afforded dark brown/orange [Rh(μ-H)(CO)(TXPB)] (**2**) in 65 % yield (Scheme 2). The $^{31}P\{^1H\}$ NMR spectrum contains a doublet located at 57.9 ppm with $^1J_{P,Rh}$ coupling of 144 Hz. The ^{11}B NMR shift for **2** is 3 ppm, indicative of 4-coordinate boron, and a hydride signal was observed at –4.05 ppm in the ^1H NMR spectrum, featuring ^{103}Rh and ^{31}P coupling (57 and 25 Hz, respectively) as well as quadrupolar broadening ($\omega_{1/2}$ ~ 103 Hz) due to coordination to boron. These data are consistent with a rhodium(I) complex bearing a hydride ligand in a bridging position between the metal and a pendant borane, and fall within the range observed for related rhodium(I) complexes (Table 1).

Scheme 2. Synthesis of [RhH(CO)(TXPB)] (**2**).

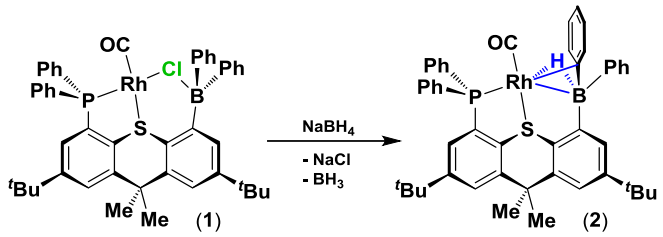

Complex	^{1}H NMR δ (ppm)	^{11}B NMR δ (ppm)	Rh–H (Å)	B–H (Å)	Rh···B (Å)	Rh–H–B (°)	Σ(E–B–E)[a] (°)	Reference
[Rh(CO)(PPh$_3$)(μ-H)(^{Ph}DPB^{Ph})]	–11.61	11.5	1.76(6)	1.24(5)	2.849	143.07	341.2(6)	[17]
[Rh(PPh$_3$)(μ-H)(^{Ph}DPB^{Ph})]	–7.6	1.9	1.65(4)	1.34(4)	2.734	132.01	337.2(6)	[17]
[Rh(PPh$_3$)(H$_3$BN(trop)$_2$}]	–6.96	–0.4	1.69(3)	1.28	2.36	104	345	[18]
[(TXPB)RhH(CO)]	–4.05	3.0	1.84(5)	1.59(6)	2.456(6)	92(2)	337.1(8)	this work
[Rh(H)$_2$(P^{t}Bu$_3$)(Tai)]	–0.7	–0.7	1.86(2)	1.24(2)	2.789	131.8	332.7(1)	[19]
[Rh(NHC)(H$_3$BN(trop)$_2$}]	–0.55	–13.2	1.74(5)	1.30	2.40	104	341	[18]
trans-[Rh(PPh$_3$)$_2$(CO){H$_3$B(ai)}]	~0.5	–15.1	2.05(2)	1.13(2)	3.083(2)	151(2)	326	[20]
[Rh(cod)(Tai)]	0.88	–2.2	1.99(2)	1.17(3)	2.971	139(2)	337.9(4)	[21]
[Rh{P(C$_7$H$_7$)$_3$}(Tp')]	0.90	–1.9	1.789(7)	1.288(7)	2.809	131.1	337.7	[22]
			1.899(7)	1.200(7)	2.829	130.0	337.0	
[Rh(COD){HBMes$_2$(O=P(OEt)$_2$NXyl)}]	2.2	–4.2	1.75(2)	1.32(2)	2.83	134	337	[14]
[Rh(cod)(^{Ph}Bai)]	4.21	–4.6	2.00(4)	1.15(4)	2.937(4)	143(5)	337.4(5)	[23]
[Rh(COD){HBCy$_2$(O=P(OEt)$_2$NXyl)}]	13.0	–8.7	1.70(2)	1.31	2.87	144	338	[15]
[Rh(cod){H$_2$B(mt)$_2$}]	not given	–5.5	2.13(3)	1.139	3.033(6)	134(2)	325	[24]
[Rh(nbd)(Tai)]	not given	–1.5	1.98(5)	1.15(2)	2.922	137.7	337.8(5)	[23]
[Rh(CO)(PPh$_3$){HB(taz)$_3$}]	not given	–5.0	2.41	1.00	3.239	139	328.8(5)	[25]
[Rh(COD){(H$_3$BPPh$_2$)$_2$CH}]	fluxional	fluxional	1.83(3)	1.32(3)	2.75	121	336	[26]

Table 1. Spectroscopic and structural data for crystallographically characterized rhodium(I) complexes featuring a single Rh–H–BR$_3$ bridging interaction. Boron and hydrogen atoms in the table refer specifically to those engaged in the Rh–H–BR$_3$ bridging interaction. Any crystallographic data not included in the journal articles was obtained from the Cambridge Structural Database. [a] Σ(E–B–E) = the sum of the angles around boron, not including the bridging hydride substituent. Abbreviations: ai = 7-azaindolyl; ^{Ph}Bai = HBPh(7-azaindolyl)$_2$; ^{Ph}DPB^{Ph} = {(*o*-Ph$_2$P)C$_6$H$_4$}$_2$BPh); mt = 2-sulfanyl-1-methylimidazolyl; NHC = C(NMe)$_2$(CMe)$_2$; Tai = B(7-azaindolyl)$_3$; taz = 4-ethyl-3-methyl-5-thioxo-1,2,4-triazolyl; Tp' = tris(3,5-dimethylpyrazolyl)hydroborate; trop = 5H-dibenzo[a,d]cyclohepten-5-yl.

X-ray quality crystals of **2**·2(C_6H_{14}) (Figure 1; Table 2) were obtained by slow diffusion of hexanes into a solution of **2** in CH_2Cl_2 at –30 °C. The solid state structure confirmed that the hydride ligand in **2** (located in the difference map) bridges between rhodium and the pendant borane of TXPB, with short Rh–H, Rh–B and Rh–C_{ipso} {C_{ipso} = C(42)} distances of 1.84(5), 2.456(6) and 2.568(5) Å, respectively; calculated (ADF, PBE, D3BJ, TZ2P, all electron, ZORA) Rh–H, Rh–B and Rh–C_{ipso} distances for **2** are 1.719, 2.434 and 2.491 Å, and the corresponding Mayer bond orders are 0.58, 0.23 and 0.27. The geometry at rhodium is distorted square planar with P–Rh–H and S–Rh–C(48) angles of 162(2)° and 157.7(2)°, respectively, and the Rh–H–B angle is 92(2)° (calcd. 102.2°). Boron is significantly pyramidalized, with the sum of the C–B–C angles equal to 337.1(8)°, but the B–H distance of 1.59(6) Å (calcd. 1.399 Å, with a Mayer bond order of 0.39) falls at the longer end of the usual range. The H–B–C angles for complex **2** are 121(2), 102(2) and 96(2)° (calcd. 112.1, 108.6 and 97.8°).

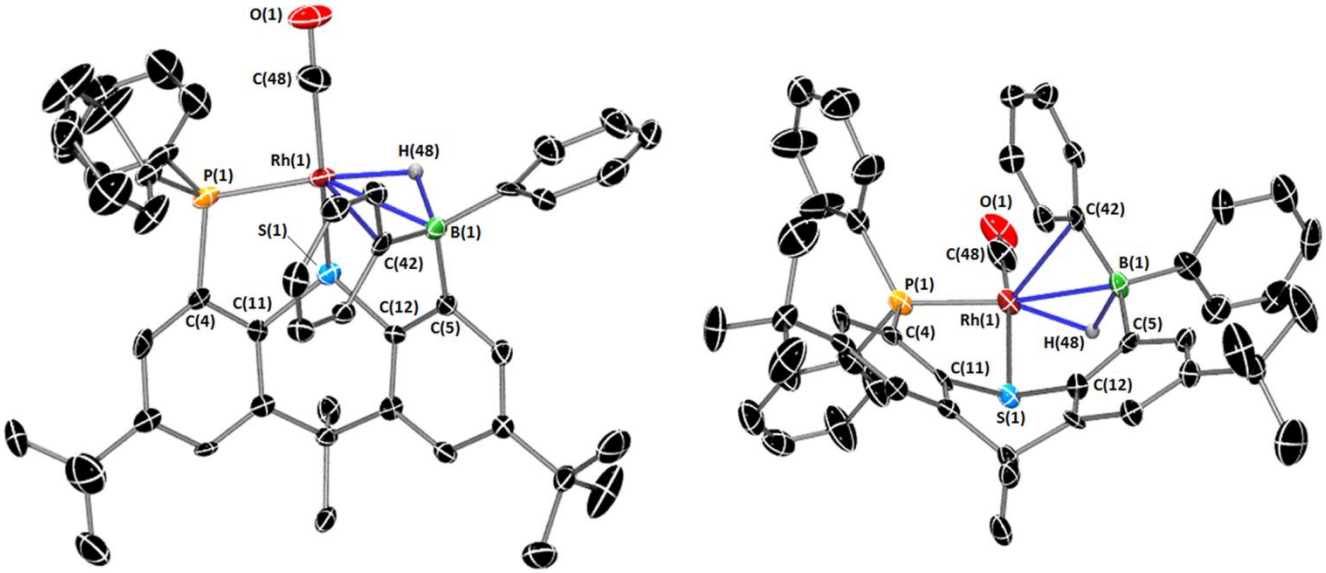

Figure 1. Two views of the X-ray crystal structure of [RhH(CO)(TXPB)]·2(C_6H_{14}) (**2**·2(C_6H_{14})). Lattice solvent and all hydrogen atoms attached to carbon are omitted for clarity. Ellipsoids are set to 50 %. Selected bond lengths [Å] and angles [°] for **2**·2(C_6H_{14}): Rh(1)–H(48), 1.84(5); Rh(1)–B(1), 2.456(6); Rh(1)–C(42), 2.568(5); Rh(1)–C(48), 1.853(6); B(1)–H(48), 1.59(6); Rh(1)–P(1), 2.261(2); Rh(1)–S(1),

2.289(1); Rh(1)–B(1)–H(48), 48(2); B(1)–Rh(1)–H(48), 40(2); Rh(1)–H(48)–B(1), 92(2); C(5)–B(1)–C(36), 111.7(5); C(5)–B(1)–C(42), 109.3(4); C(36)–B(1)–C(42), 116.1(5); S(1)–Rh(1)–C(48), 157.7(2); P(1)–Rh(1)–H(48), 162(2); P(1)–Rh(1)–B(1), 146.2(2); P(1)–Rh(1)–C(42), 114.8(1); S(1)–C(12)–C(5)–B(1), 20.3(7).

The Rh–B distance in **2** is remarkably short, even compared with related [Rh(CO)(TXPB)][PF_6] which features η^2*BC*-coordination of a *B*-phenyl group to rhodium; the Rh–B and Rh–C_{ipso} distances in [Rh(CO)(TXPB)][PF_6] are 2.557(3) and 2.362(2), respectively (c.f. 2.456(6) and 2.568(5) Å in **2**). However, a similar bonding situation, involving an M–H–B bridging interaction with particularly short M–B and M–H bonds, a long B–H distance, and an acute M–H–B angle (but without a short M–C_{ipso} contact), was recently reported for [PtH(μ-H)(FcPPB)] (Figure 2), with calculated Pt–B, Pt–H and B–H distances of 2.524, 1.386 and 1.686 Å (the covalent radii of Rh and Pt are 1.42 and 1.36 Å, respectively), and a Pt–H–B angle of 110.1°.[27] Additionally, very short Rh–B distances (2.36-2.40 Å) were observed in [Rh(L)($H_3BN(trop)_2$}] {L = PPh_3 or $C(NMe)_2(CMe)_2$}, accompanied by short Rh–H bonds (1.69-1.74 Å) and an acute Rh–H–B angle (104°),[18] perhaps in this case due to constraints imposed by formation of a 4-membered N–B–H–Rh ring with a short Rh–N bond (2.09 Å).

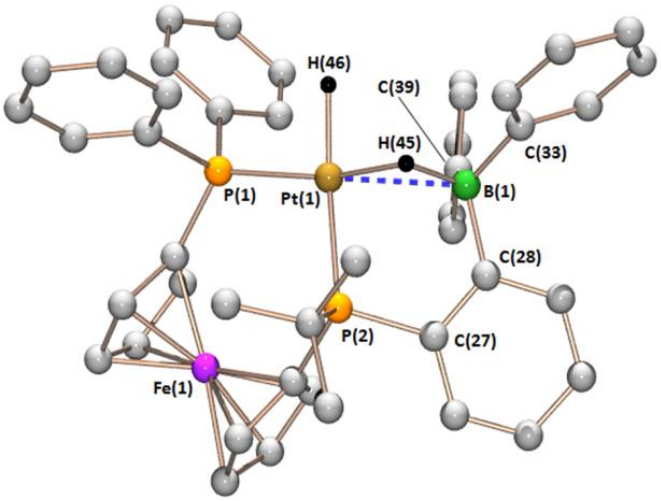

Figure 2. Calculated structure of [PtH(μ-H)(FcPPB)] with most hydrogen atoms omitted for clarity. Reproduced with permission from John Wiley and Sons. The shortest Pt–C_{ipso} distance is 2.806 Å.[11]

Complex **2** possesses the longest Rh–P bond length in the series of rhodium TXPB complexes (2.261(2) Å in **2** vs. 2.196(2)–2.224(1) Å in **1** and **3**-**5**) and the smallest $^{1}J_{P,Rh}$ coupling constant (144 Hz in **2** vs. 161–167 Hz in **1** and **3**-**5**). However, the Rh–S bond length of 2.289(1) Å in **2** is shorter than the Rh–S distances in **1** and **3**-**5** (2.300(1)–2.405(1) Å), suggesting that the Rh–S and Rh–P distances are strongly influenced by the structural requirements of the ambiphilic ligand framework, especially those stemming from the much shorter Rh–B distance in **2** than in **1** and **3**-**5** {2.456(6) Å vs. 3.23-3.65 Å}.[6]

At 20 °C, each of the two *B*-phenyl rings in **2** gave rise to just three signals in the ^{1}H NMR spectrum. However, the *ortho*-protons of one *B*-phenyl ring de-coalesced at –67 °C, indicating that the interaction between rhodium and the *ipso* carbon atom of one of the *B*-phenyl rings is maintained on the NMR timescale at low temperature. The CO stretching frequency for **2** is 1984 cm^{-1} in Nujol versus 2006 cm^{-1} in CH_2Cl_2, suggesting the accessibility of room temperature solution structures in which the Rh–C_{ipso} or Rh–H interaction is not maintained to the same extent. The CO stretching frequency for **2** in Nujol (*vide infra*) is substantially lower than those of [RhX(CO)(TXPB)] (X = F (**3**), Cl (**1**), Br (**4**), I (**5**); ν(CO)(Nujol) = 2004-2013 cm^{-1}),[6] indicating that the hydride ligand in **2** remains a strong donor relative to a halide ligand, despite partial abstraction by the borane, and/or reflecting the presence of a Rh–C_{ipso} interaction in **2** that is absent in **1** and **3**-**5**.

Structure	**2**·2(C_6H_{14})	**6**·toluene
Formula	$C_{60}H_{77}BOPRhS$	$C_{54}H_{56}BBr_2NiPS$
Formula wt	990.96	997.34
T (K)	100(2)	100(2)
Cryst. Syst.	Triclinic	Orthorhombic
Space Group	*P*–1	*P*bn2_1
a (Å)	10.907(2)	9.0175(15)
b (Å)	13.536(3)	21.625(4)
c (Å)	16.766(4)	24.361(4)

α [deg]	96.447(4)	90
β [deg]	93.892(5)	90
γ [deg]	91.612(6)	90
Volume (Å^3)	2452.3(9)	4750(1)
Z	2	4
Crystal Size (mm^3)	0.20×0.08×0.02	0.29×0.13×0.06
No. of reflns collected	26269	41712
No. of indep Reflns	8972	8162
θ range for collection (°)	1.87–25.44	1.88–26.43
Completeness to θ Max (%)	98.8	99.7
Absorption Correction	Numerical	Numerical
GOF on F^2	0.841	0.986
Final R_1 [$I > 2\sigma(I)$] (%)	6.08	4.22

Table 2. Crystallographic data collection and refinement parameters for compounds **2** and **6**.

A nickel(II) μ-Bromide Complex:

Reaction of TXPB with [$NiBr_2(dme)_2$] (dme = 1,2-dimethoxyethane) in tetrahydrofuran gave a red-purple solution from which light purple [$NiBr_2$(TXPB)] (**6**) was isolated in 64 % yield (Scheme 3). The room temperature ^{11}B NMR chemical shift for **6** is 23 ppm, which is shifted to lower frequency relative to that of free TXPB (69 ppm), and is in good agreement with that of [RhBr(CO)(TXPB)] (**4**; 27 ppm), which also features a bromide ligand bridging between the metal and the borane.[6] A ^{31}P NMR signal could not be detected for **6** at room temperature, but low temperature ^{31}P{^{1}H} NMR spectroscopy revealed a broad ^{31}P NMR signal at –20 °C (53 ppm, $\omega_{1/2}$ = 165 Hz) which sharpened at lower temperatures (^{31}P δ = 53.6 ppm at –67 °C, Figure 3). By contrast, the ^{1}H and ^{13}C NMR chemical shifts for **6** were reasonably sharp, and in the usual range for a diamagnetic compound.

Scheme 3. Synthesis of [$NiBr_2$(TXPB)] (**6**).

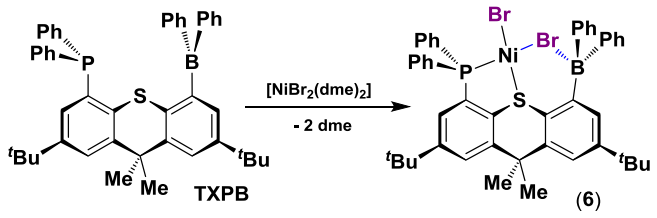

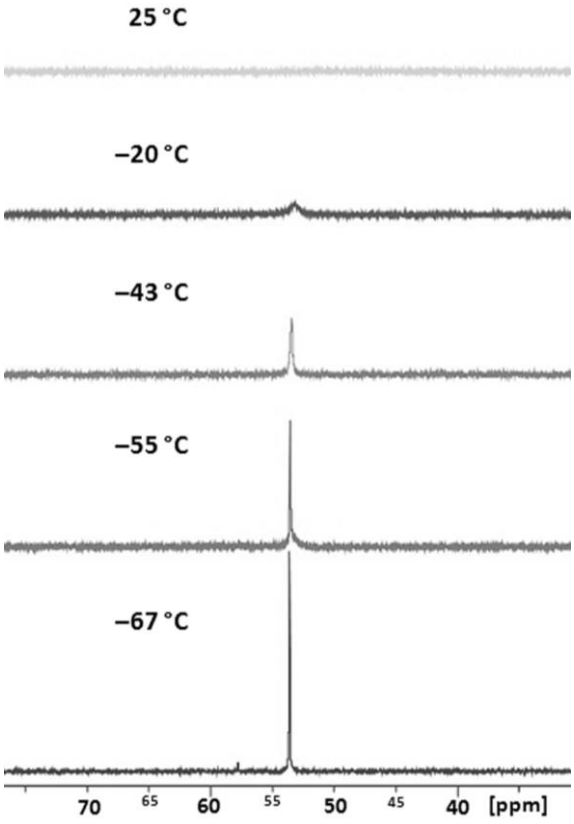

Figure 3. Variable temperature $^{31}P\{^{1}H\}$ NMR spectra of **6** (CD_2Cl_2, 203 MHz).

Similar spectroscopic characteristics have been reported by Jean and Le Floch for [$NiBr_2$(DMP-Xantphos)] (DMP-Xantphos = 4,5-di(3,4-dimethylphospholyl)-9,9-dimethylthioxanthene), which gave rise to NMR silent ^{1}H and ^{31}P NMR spectra at room temperature. The ^{1}H NMR spectrum remained broad and ill-defined even at –80 °C. By contrast, at –40 °C a broadened ^{31}P NMR signal emerged ($\omega_{1/2}$ = 840 Hz), sharpening as the temperature was decreased to –80 °C ($\omega_{1/2}$ = 98 Hz). Moreover, cooling a solution of [$NiBr_2$(DMP-Xantphos)] in dichloromethane to –80 °C resulted in a colour change from dark blue to pale violet, indicative of a change in the relative proportions of d^8 tetrahedral and square planar isomers, with the latter favored at low temperature.[28] The spectroscopic data for **6** are consistent with an analogous equilibrium between a square planar and a tetrahedral isomer at room temperature and above, although room temperature Evans magnetic measurements[29] were unable to detect the presence of a paramagnetic

isomer, and solutions of **6** did not undergo a significant colour change between –80 and 60 °C, indicating that any tetrahedral isomer is present in low concentration.

An X-ray crystal structure of **6** (Figure 4, Table 2) revealed a square-planar geometry with P–Ni–Br(1) and S–Ni–Br(2) bond angles of 175.86(5) and 168.16(5)°, respectively, and a C(12)–C(5)–B–Br torsion angle of –53.1(6)°. A strong B–Br interaction is also evident in the solid-state structure of **6**, based on the short B–Br(1) bond length of 2.311(6) Å, and the extent of pyramidalization at boron (Σ(C–B–C) = 344.5(7)°). In the solid state structure of rhodium complex **4** {for the molecule in the unit cell with a negative C(12)–C(5)–B–Br torsion angle (–43°); i.e. a structure analogous to that of **6**}, the B–Br distance of 2.267(9) Å is shorter than that in **6**, and boron is more pyramidalized {Σ(C–B–C) = 339(1) °}. These differences can perhaps be attributed to the lower oxidation state of rhodium(I) vs nickel(II), rendering the bromide ligands in rhodium complex **4** more basic towards external electrophiles. To the best of our knowledge, complexes **4** and **6** are the only crystallographically characterized complexes in which a bromide co-ligand bridges between a metal centre and the pendant borane of an ambiphilic ligand.

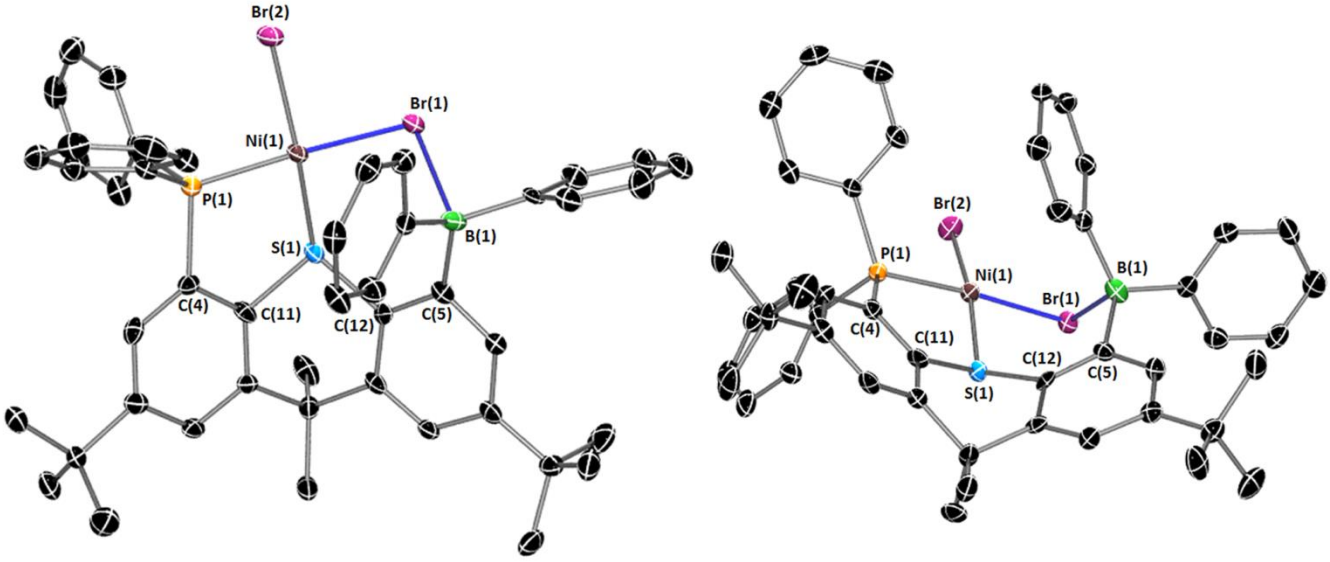

Figure 4. Two different views of the X-ray crystal structure of [$NiBr_2$(TXPB)]·toluene (**6**·toluene). Lattice solvent and hydrogen atoms are omitted for clarity. Ellipsoids are set to 50 %. Selected bond lengths [Å] and angles [°] for **6**·toluene: Ni(1)–Br(1), 2.3511(8); Ni(1)–Br(2), 2.2968(8); Ni(1)–P(1),

2.152(1); Ni(1)–S(1), 2.155(1); B(1)–Br(1), 2.311(6); P(1)–Ni(1)–Br(1), 175.86(5); S(1)–Ni(1)–Br(2), 168.16(5); Ni(1)–Br(1)–B(1), 91.9(2); C(5)–B(1)–C(36), 114.1(4); C(5)–B(1)–C(42), 113.5(4); C(36)–B(1)–C(42), 116.9(4); S(1)–C(12)–C(5)–B(1), 20.4(7).

The Ni–Br(1) and Ni–Br(2) bond lengths in **6** are 2.3522(8) and 2.2968(8) Å, where Br(1) and Br(2) are *trans* to the phosphine and thioether moieties, respectively {Br(1) occupies the bridging position between Ni and B}. The weaker Ni–Br(1) bond, relative to Ni–Br(2), is primarily as a consequence of the greater *trans* influence of the phosphine versus the thioether donor of TXPB, rather than partial abstraction of bromide by the borane. For comparison, the M–X bonds *trans* to the phosphine are 0.042–0.083 Å longer than the M–X bonds *trans* to the sulfur donor in the following complexes: [MX_2(TXPB)] (M = Pd, X = Cl; M = Pt, X = Cl, I), and borane-free [MX_2(TXPH)] (M = Pd, X = Cl; M = Pt, X = I; TXPH = 2,7-di-*tert*-butyl-4-diphenylphosphino-9,9-dimethylthioxanthene),[7] [$NiBr_2${κ^2*PS*-(Ph_2P)N{P(S)Ph_2}(*p*-C_6H_4)SMe}],[30] and *cis*-[$PtBr_2${1-(PPh_2)-8-(SPh)-$C_{10}H_6$}].[31]

Summary and Conclusions

The previously reported series of [Rh(X)(CO)(TXPB)] (X = F, Cl, Br, I) complexes has been extended to include [Rh(μ-H)(CO)(TXPB)] (**2**), in which rhodium is bound to the bridging hydride ligand, boron, and the *ipso* carbon atom of a *B*-phenyl ring, with calculated Mayer bond orders of 0.58, 0.23 and 0.27, respectively. Notable features of **2** are an uncommonly acute Rh–H–B angle, a particularly short Rh–B contact, an elongated B–H bond, and a Rh*H*BR_3 ^{1}H NMR signal indicative of appreciable hydridic character. These features indicate a bonding description intermediate between the following extremes: (a) an η^2BC-coordinated borane ligand that also interacts, via boron, with a hydride co-ligand, and (b) a σ-interaction between rhodium and a hydroborate anion, with an additional η^1-interaction between rhodium and the *ipso* carbon atom of one of the *B*-phenyl rings.

The second structurally characterized example of an ambiphilic ligand featuring a M–Br–BR_3 interaction is also reported. This complex, [NiBr(μ-Br)(TXPB)] (**6**), is square planar in the solid state with a strong Br–BR_3 interaction. However, the absence of a solution ^{31}P NMR signal at room temperature, but emergence of a sharp signal at low temperature, suggest that in solution at room temperature and above, square planar **6** exists in equilibrium with a tetrahedral isomer.

Overall, complexes **2** and **6** expand the range of reported TXPB ligand complexes, providing the first examples of a TXPB complex with a bridging hydride ligand, and the first example of a nickel(II) TXPB complex. These complexes contribute to our understanding of metal–(co-ligand)–Lewis acid interactions, which is essential to facilitate the rational development of future catalytic cycles involving ambiphilic ligands in combination with hydride or halide ligands, both of which are commonplace in organometallic and coordination chemistry.

Experimental Section

General Details. An argon-filled MBraun UNIlab glove box equipped with a −30 °C freezer was employed for the manipulation and storage of the TXPB ligand and its complexes, and reactions were performed on a double manifold high vacuum line using standard techniques.[32] A Fisher Scientific Ultrasonic FS-30 bath was used to sonicate reaction mixtures where indicated. Residual oxygen and moisture was removed from the argon stream by passage through an Oxisorb-W scrubber from Matheson Gas Products.

Toluene was initially dried and distilled at atmospheric pressure from Na, while hexanes and tetrahydrofuran (THF) were initially dried and distilled at atmospheric pressure from Na/benzophenone. Unless otherwise noted, all proteo solvents were stored over an appropriate drying agent (toluene, THF = Na/Ph_2CO; hexanes = Na/Ph_2CO/tetraglyme) and introduced to reactions via vacuum transfer with condensation at −78 °C. Deuterated solvents (ACP Chemicals) were dried over CaH_2 (CD_2Cl_2). $NaBH_4$ was purchased from Sigma-Aldrich, and anhydrous $NiBr_2$ was purchased from Strem Chemicals; both reagents were stored under argon.

The TXPB ligand,[33] [Rh(μ-Cl)(CO)(TXPB)][8] and $[NiBr_2(dme)_2]$[34] were prepared according to literature procedures. IR Spectra were recorded on a Thermo Scientific Nicolet 6700 FTIR spectrometer. Combustion elemental analyses were performed on a Thermo EA1112 CHNS/O analyzer. NMR spectroscopy (^1H, $^{13}C\{^1H\}$, ^{11}B, $^{31}P\{^1H\}$, DEPT-135, uDEFT, COSY, HSQC, HMBC) was performed on Bruker DRX-500 and AV-600 spectrometers. All ^1H NMR and ^{13}C NMR spectra were referenced relative to $SiMe_4$ through a resonance of the employed deuterated solvent or proteo impurity of the solvent (CD_2Cl_2); 5.32 ppm for ^1H NMR, and 54.0 ppm for ^{13}C NMR. ^{11}B and $^{31}P\{^1H\}$ NMR spectra were referenced using an external standard of $BF_3(OEt_2)$ (0.0 ppm) and 85% H_3PO_4 in D_2O (0.0 ppm), respectively. Temperature calibration was performed using a d_4-methanol sample, as outlined in the Bruker VTU user manual. Herein, numbered proton and carbon atoms refer to the positions of the thioxanthene backbone in the TXPB ligand.[7] Inequivalent phenyl rings on boron and phosphorus are

labeled A and B so that the proton and carbon resonances belonging to a single phenyl ring can be identified. We did not identify which *P*-phenyl ring gives rise to the signals labeled A or B, however the signals corresponding to the η^2-coordinated *B*-phenyl ring is labeled as B in complex **2**.

X-ray crystallographic analyses were performed on suitable crystals coated in Paratone oil and mounted on a SMART APEX II diffractometer with a 3 kW Sealed tube Mo generator in the McMaster Analytical X-Ray (MAX) Diffraction Facility. In all cases, non-hydrogen atoms were refined anisotropically and hydrogen atoms were generated in ideal positions and then recalculated with each cycle of refinement, with the exception being H(48) in **2**·2(C_6H_{14}), which was located in the difference map and refined isotropically. Two molecules of hexanes in **2**·2(C_6H_{14}) and one molecule of toluene in **6**·toluene were SQUEEZED from the lattice of each respective structure due to unresolveable disorder.[35] The Evans measurements[29] for complex **6** were performed at 298 K without spinning on a Bruker DRX-500 MHz spectrometer, and the solvent was an approximate 1:40 mixture of toluene and d_8-toluene. The sample solution was contained within a medium wall 4mm O.D. Suprasil EPR tube with a teflon valve (Wilmad LVP tube). This quartz tube was anchored (by a ring of teflon tape) within a 5 mm O.D. thin wall borosilicate NMR tube (4.2 mm I.D.) containing pure solvent.

[Rh(μ-H)(CO)(TXPB)] (2): THF (10 mL) was condensed into a 100 mL round bottom flask containing [RhCl(CO)(TXPB)] (165 mg, 0.193 mmol) and $NaBH_4$ (7.30 mg, 0.193 mmol) through the use of a dry ice/acetone bath. The reaction was left to stir overnight at room temperature, over which time the initially yellow solution progressively became dark brown/orange. The reaction mixture was then evaporated to dryness *in vacuo* to yield a red/brown oily residue. Toluene (20 mL) was added to the crude residue and the resulting mixture was sonicated for 15 minutes and filtered to remove any NaCl (which was washed with 10 mL of toluene). The dark brown/orange filtrate was evaporated to dryness *in vacuo*, again yielding a red/orange oily residue, to which hexanes (20 mL) were added; the crude hexanes solution was sonicated for 15 minutes, allowing for [RhH(CO)(TXPB)] to precipitate from solution as a light brown powder. The hexanes solution was filtered and the collected product was washed with hexanes (2 × 10 mL) then dried

in vacuo. Yield = 102 mg (65 %). X-ray quality crystals were obtained by slow diffusion of hexanes (~10 mL) into a solution of **1** (~30 mg) in CH_2Cl_2 (~3 mL) at –30 °C. **^{1}H NMR (600 MHz, CD_2Cl_2, 298 K):** δ 7.70 (s, 1H, CH^1), 7.63–7.59 (m, 4H, *o*-PPh_2 A, *o*-BPh_2 A), 7.53–7.48 (m, 3H, *m*+*p*-PPh_2 A), 7.43 (s, 1H, CH^8), 7.40 (t, $^3J_{H,H}$ 7 Hz, 1H, *p*-PPh_2 B), 7.30–7.28 (m, 4H, *m*-PPh_2 B, *m*-BPh_2 A), 7.18 (t, $^3J_{H,H}$ 7 Hz, 1H, *p*-BPh_2 A), 7.15–7.14 (m, 2H, CH^3, CH^6), 7.01–6.93 (m, 5H, *o*-PPh_2 B, *m*+*p*-BPh_2 B), 6.69 (t, $^3J_{H,H}$ 7 Hz, 2H, *o*-BPh_2 B), 2.12, 1.59 (2×s, 6H, CMe_2), 1.24, 1.20 (2×s, 18H, 2×CMe_3), –4.05 (dd, $^1J_{H,Rh}$ 57 Hz, $^2J_{H,P}$ 25 Hz, 1H, Rh–*H*–B). **^{13}C NMR (151 MHz, CD_2Cl_2, 298 K):** δ 188.7 (dd, $^1J_{C,Rh}$ 77 Hz, $^2J_{C,P}$ 16 Hz, Rh–*C*O), 155.7 (broad s, C^5), 153.9 (broad s, *ipso*-BPh_2 A), 153.5 (d, $^3J_{C,P}$ 6 Hz, C^2), 151.2 (s, C^7), 145.7 (d, $^3J_{C,P}$ 13 Hz, C^{10}), 143.9 (broad s, *ipso*-BPh_2 B), 141.0 (s, C^{13}), 138.6 (d, $^2J_{C,P}$ 26 Hz, C^{11}), 137.1 (s, *o*-BPh_2 B), 136.6 (d, $^1J_{C,P}$ 49 Hz, C^4), 135.7 (s, *o*-BPh_2 A), 133.7 (d, $^2J_{C,P}$ 13 Hz, *o*-PPh_2 B), 133.2 (d, $^1J_{C,P}$ 50 Hz, *ipso*-PPh_2 A), 133.2 (d, $^2J_{C,P}$ 13 Hz, *o*-PPh_2 A), 132.0 (d, $^1J_{C,P}$ 51 Hz, *ipso*-PPh_2 B), 131.9 (d, $^4J_{C,P}$ 4 Hz, C^{12}), 131.4 (s, *p*-PPh_2 B), 131.3 (s, *p*-PPh_2 A), 130.5 (s, C^6), 129.5 (d, $^3J_{C,P}$ 11 Hz, *m*-PPh_2 A), 128.7 (d, $^3J_{C,P}$ 11 Hz, *m*-PPh_2 B), 128.2 (s, C^3), 127.4 (s, *m*-BPh_2 A), 126.6 (s, *m*-BPh_2 B), 125.7 (s, *p*-BPh_2 B), 125.5 (s, *p*-BPh_2 A), 125.4 (s, C^1), 119.8 (s, C^8), 43.2 (s, *C*Me$_2$), 35.6, 35.2 (2×s, 2×*C*Me$_3$), 31.7, 31.4 (2×s, 2×CMe_3), 26.6, 25.4 (2×s, CMe_2). **^{31}P{^{1}H} NMR (203 MHz, CD_2Cl_2, 298 K):** δ 57.9 (d, $^2J_{P,Rh}$ 144 Hz). **^{11}B NMR (161 MHz, CD_2Cl_2, 298 K):** δ 3 (broad s, $\omega_{1/2}$ ~ 1000 Hz). IR: ν(CO) = 1984 cm^{-1} (nujol), 2006 cm^{-1} (CH_2Cl_2). A satisfactory elemental analysis was not obtained, but the NMR spectra of **2** (provided in the supporting information) indicate that compound **2** was obtained in pure form.

[NiBr(μ-Br)(TXPB)] (6): THF (50 mL) was condensed into a 100 mL round bottom flask containing [$NiBr_2(DME)_2$] (88.7 mg, 0.223 mmol) and TXPB (153 mg, 0.223 mmol) through the use of a dry ice/acetone bath. The reaction was left to stir overnight at room temperature, over which time the initially yellow solution progressively became purple/red. The reaction mixture was then evaporated to dryness *in vacuo* leaving behind a dark purple/red, oily residue. Toluene (50 mL) was added to the crude residue and the resulting mixture was sonicated for 15 minutes and filtered to remove any unreacted [$NiBr_2(dme)_2$] (which was washed with 10 mL of toluene). The dark purple/red filtrate was evaporated to

dryness *in vacuo*, yielding a dark purple solid, to which hexanes (30 mL) were added; the crude hexanes solution was sonicated for 15 minutes, allowing for [$NiBr_2$(TXPB)] to precipitate from solution as a light purple powder. The hexanes solution was filtered and the collected product was washed with hexanes (2 × 10 mL) then dried *in vacuo*. Yield = 129 mg (64 %). X-ray quality crystals were obtained by slow diffusion of hexanes (~10 mL) into a solution of **1** (~30 mg) in toluene (~3 mL) at –30 °C. **^{1}H NMR (500 MHz, CD_2Cl_2, 298 K):** δ 7.77 (s, 1H, C*H*^{1}), 7.64 (s, 1H, C*H*^{8}), 7.55–7.50 (m, 6H, *m*+*p*-P*Ph*$_2$), 7.46–7.43 (m, 4H, *o*-P*Ph*$_2$), 7.35 (d, $^3J_{H,H}$ 7 Hz, 4H, *o*-B*Ph*$_2$), 7.11 (t, $^3J_{H,H}$ 7 Hz, 4H, *m*-B*Ph*$_2$), 7.07–7.03 (m, 3H, C*H*^{3}, *p*-B*Ph*$_2$), 6.97 (s, 1H, C*H*^{6}), 1.91 (s, 6H, C*Me*$_2$), 1.21, 1.16 (2×s, 18H, 2×C*Me*$_3$). **^{13}C NMR (126 MHz, CD_2Cl_2, 298 K):** δ 154.6 (s, *C*^{7}), 150.7 (app. s, *C*^{2}), 148.3 (broad s, *ipso*-B*Ph*$_2$), 146.3 (s, *C*^{13}), 142.8 (broad s, *C*^{10}), 136.6 (app. s, *C*^{11}), 136.4 (s, *o*-B*Ph*$_2$), 135.2 (s, *m*-P*Ph*$_2$), 132.9 (s, *C*^{6}), 132.5 (s, *p*-P*Ph*$_2$), 129.0 (s, *o*-P*Ph*$_2$), 128.7 (s, *C*^{3}), 128.0 (s, *C*^{12}), 127.3 (s, *m*-B*Ph*$_2$), 127.3 (s, *m*-B*Ph*$_2$), 126.7 (s, *C*^{1}), 121.9 (s, *C*^{8}), 43.0 (s, *C*Me$_2$), 35.5, 35.0 (2×s, 2×*C*Me$_3$), 31.3 (2×s, 2×C*Me*$_3$), 26.7 (s, C*Me*$_2$). **^{31}P{^{1}H} NMR (203 MHz, CD_2Cl_2, 206 K):** δ 53.6 (s). **^{11}B NMR (161 MHz, CD_2Cl_2, 298 K):** δ 23 (broad s, $\omega_{1/2}$ ~ 2200 Hz). Anal. Calcd. For $C_{47}H_{48}BBr_2NiPS$ (%): C, 62.36; H, 5.34. Found: C, 62.49; H, 5.70.

DFT Calculations: The structure of **2** was fully optimized with the ADF DFT package (SCM, version 2013.01).[36] Calculations were conducted using the zero-order regular approximation (ZORA)[37] for relativistic effects, and 1996 Perdew-Burke-Ernzerhof exchange and correlation for the GGA part of the density functional (PBE),[38] combined with Grimme's DFT-D3-BJ dispersion correction.[39] All calculations were restricted gas-phase calculations. Preliminary geometry optimizations were conducted with frozen cores corresponding to the configuration of the preceding noble gas (core = medium) using a double-ζ basis set with one polarization function (DZP). These structures were further refined using an all-electron TZ2P basis set (the size and quality of ADF basis sets increases in the order SZ < DZ < DZP < TZP < TZ2P < QZ4P) and an integration value of 7. An analytical frequency calculation showed no imaginary frequencies. Visualization of the computational results was performed using the ADF-GUI (SCM) or Discovery Studio Visualizer (Accelrys).

ASSOCIATED CONTENT

Supporting Information. General X-ray crystal structure data and refinement details for **2**.2C_6H_{14} and **6**.toluene, NMR spectra for **2** and **6**, and DFT-calculated structure and coordinates for **2**.

ACKNOWLEDGMENT

D.J.H.E. thanks NSERC of Canada for a Discovery Grant and B.E.C. thanks the Government of Canada for an NSERC PGS-D scholarship.

REFERENCES

(1) Bonanno, J. B.; Henry, T. P.; Wolczanski, P. T.; Pierpont, A. W.; Cundari, T. R. *Inorg. Chem.* **2007**, *46*, 1222.

(2) Complexes thought to be [$(Et_3P)_3Pt\{BF_2(C_6F_5)\}$] and [$(Cy_3P)_2Pt\{BF_2(C_6H_3(CF_3)_2\text{-}3,5)\}$] have been generated in solution: Bauer, J.; Braunschweig, H.; Dewhurst, R. D.; Radacki, K. *Chem. Eur. J.* **2013**, *19*, 8797.

(3) Hill, A. F.; Owen, G. R.; White, A. J. P.; Williams, D. J. *Angew. Chem. Int. Ed.* **1999**, *38*, 2759.

(4) (a) Amgoune, A.; Bouhadir, G.; Bourissou, D. *Top. Curr. Chem.* **2013**, *334*, 281. (b) Bouhadir, G.; Amgoune, A.; Bourissou, D. *Adv. Organomet. Chem.* **2010**, *58*, 1.

(5) (a) Fontaine, F.-G.; Boudreau, J.; Thibault, M. H. *Eur. J. Inorg. Chem.* **2008**, 5439. (b) Emslie, D. J. H.; Cowie, B. E.; Kolpin, K. B. *Dalton Trans.* **2012**, *41*, 1101.

(6) Cowie, B. E.; Emslie, D. J. H.; Jenkins, H. A.; Britten, J. F. *Inorg. Chem.* **2010**, *49*, 4060.

(7) D. J. H. Emslie; B. E. Cowie; S. R. Oakley; N. L. Huk; H. A. Jenkins; L. E. Harrington; Britten, J. F. *Dalton Trans.* **2012**, *41*, 3523

(8) Oakley, S. R.; Parker, K. D.; Emslie, D. J. H.; Vargas-Baca, I.; Robertson, C. M.; Harrington, L. E.; Britten, J. F. *Organometallics* **2006**, *25*, 5835.

(9) (a) Harman, W. H.; Peters, J. C. *J. Am. Chem. Soc.* **2012**, *134*, 5080. (b) MacMillan, S. N.; Harman, W. H.; Peters, J. C. *Chem. Sci.* **2014**, *5*, 590.

(10) Fong, H.; Moret, M. E.; Lee, Y.; Peters, J. C. *Organometallics* **2013**, *32*, 3053.

(11) Cowie, B. E.; Emslie, D. J. H. *Chem. Eur. J.* **2014**, *20*, 16899.

(12) Ostapowicz, T. G.; Merkens, C.; Holscher, M.; Klankermayer, J.; Leitner, W. *J. Am. Chem. Soc.* **2013**, *135*, 2104.

(13) Baker, R. T.; Calabrese, J. C.; Westcott, S. A.; Marder, T. B. *J. Am. Chem. Soc.* **1995**, *117*, 8777.

(14) Drover, M. W.; Bowes, E. G.; Love, J. A.; Schafer, L. L. *Organometallics* **2017**, *36*, 331.

(15) Drover, M. W.; Schafer, L. L.; Love, J. A. *Angew. Chem. Int. Ed.* **2016**, *55*, 3181.

(16) Jana, R.; Blacque, O.; Jiang, Y. F.; Berke, H. *Eur. J. Inorg. Chem.* **2013**, 3155.

(17) Kameo, H.; Nakazawa, H. *Organometallics* **2012**, *31*, 7476.

(18) Muller, F.; Trincado, M.; Pribanic, B.; Vogt, M.; Grutzmacher, H. *J. Organomet. Chem.* **2016**, *821*, 154.

(19) Tsoureas, N.; Kuo, Y.-Y.; Haddow, M. F.; Owen, G. R. *Chem. Commun.* **2011**, *47*, 484.

(20) Wagler, J.; Hill, A. F. *Organometallics* **2008**, *27*, 2350.

(21) Tsoureas, N.; Owen, G. R.; Hamilton, A.; Orpen, A. G. *Dalton Trans.* **2008**, 6039.

(22) Herberhold, M.; Eibl, S.; Milius, W.; Wrackmeyer, B. *Z. Anorg. Allg. Chem.* **2000**, *626*, 552.

(23) Tsoureas, N.; Bevis, T.; Butts, C. P.; Hamilton, A.; Owen, G. R. *Organometallics* **2009**, *28*, 5222.

(24) Crossley, I. R.; Hill, A. F.; Humphrey, E. R.; Smith, M. K. *Organometallics* **2006**, *25*, 2242.

(25) Blagg, R. J.; Charmant, J. P. H.; Connelly, N. G.; Haddow, M. F.; Orpen, A. G. *Chem. Commun.* **2006**, 2350.

(26) Blug, M.; Grunstein, D.; Alcaraz, G.; Sabo-Etienne, S.; Le Goff, X. F.; Le Floch, P.; Mezailles, N. *Chem. Commun.* **2009**, 4432.

(27) Cordero, B.; Gómez, V.; Platero-Prats, A. E.; Revés, M.; Echeverría, J.; Cremades, E.; Barragán, F.; Alvarez, S. *Dalton Trans.* **2008**, 2832.

(28) Mora, G.; van Zutphen, S.; Klemps, C.; Ricard, L.; Jean, Y.; Le Floch, P.; Bernache-Assollant, D. *Inorg. Chem.* **2007**, *46*, 10365.

(29) (a) Evans, D. F. *J. Chem. Soc.* **1959**, 2003. (b) Schubert, E. M. *J. Chem. Educ.* **1992**, *69*, 62.

(30) Ghisolfi, A.; Fliedel, C.; Rosa, V.; Monakhov, K. Y.; Braunstein, P. *Organometallics* **2014**, *33*, 2523.

(31) Gibson, V. C.; Long, N. J.; White, A. J. P.; Williams, C. K.; Williams, D. J.; Fontani, M.; Zanello, P. *J. Chem. Soc. Dalton Trans.* **2002**, 3280.

(32) Burger, B. J.; Bercaw, J. E., Vacuum Line Techniques for Handling Air-Sensitive Organometallic Compounds. In *Experimental Organometallic Chemistry - A Practicum in Synthesis and Characterization*, American Chemical Society: Washington D.C., 1987; Vol. 357, p 79.

(33) Emslie, D. J. H.; Blackwell, J. M.; Britten, J. F.; Harrington, L. E. *Organometallics* **2006**, *25*, 2412.

(34) Kermagoret, A.; Braunstein, P. *Organometallics* **2008**, *27*, 88.

(35) Sluis, P. V. D.; Spek, A. L. *Acta Crystallogr.* **1990**, *A46*, 194.

(36) Fraenkel, G.; Chow, A.; Winchester, W. R. *J. Am. Chem. Soc.* **1990**, *112*, 1382.

(37) ADF2010 . (a) Velde, G. t.; Bickelhaupt, F. M.; Gisbergen, S. J. A. v.; Guerra, C. F.; Baerends, E. J.; Snijders, J. G.; Ziegler, T. J. *J. Comput. Chem.* **2001**, *22*, 931. (b) Guerra, C. F.; Snijders, J. G.; Velde, G. t.; Baerends, E. *J. Theor. Chem. Acc.* **1998**, *99*, 391.

(38) (a) Lenthe, E. v.; Baerends, E. J.; Snijders, G. J. *J. Chem. Phys.* **1994**, *101*, 9783. (b) Lenthe, E. v.; Baerends, E. J.; Snijders, J. G. *J. Chem. Phys.* **1993**, *99*, 4597. (c) Lenthe, E. v.; Ehlers, A.; Baerends, E. J. *J. Chem. Phys.* **1999**, *110*, 8943. (d) Lenthe, E. v.; Leeuwen, R. v.; Baerends, E. J.; Snijders, J. G. *Int. J. Quantum Chem.* **1996**, *57*, 281. (e) Lenthe, E. v.; Snijders, J. G.; Baerends, E. J. *J. Chem. Phys.* **1996**, *105*, 6505.

(39) Perdew, J. P.; Burke, K.; Ernzerhof, M. *Phys. Rev. Lett.* **1996**, *77*, 3865.

For Table of Contents Use Only

M–H–BR_3 and M–Br–BR_3 Interactions in Rhodium and Nickel Complexes of an Ambiphilic Phosphine-Thioether-Borane Ligand

Bradley E. Cowie and David J. H. Emslie*

TOC Graphic: